

# Reaction Pathways in $\text{Ca}(\text{BH}_4)_2\text{-NaNH}_2$ and $\text{Mg}(\text{BH}_4)_2\text{-NaNH}_2$ Hydrogen-Rich Systems

Fabrice Morelle,<sup>†</sup> Lars H. Jepsen,<sup>‡</sup> Torben R. Jensen,<sup>‡</sup> Manish Sharma,<sup>§</sup> Hans Hagemann,<sup>§</sup> and Yaroslav Filinchuk<sup>\*,†</sup>

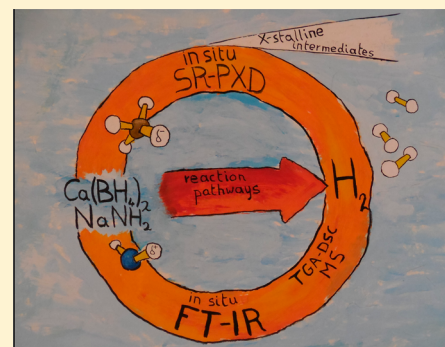
<sup>†</sup>Institute of Condensed Matter and Nanosciences, Université Catholique de Louvain, Place L. Pasteur 1, 1348 Louvain-la-Neuve, Belgium

<sup>‡</sup>Center for Materials Crystallography, Interdisciplinary Nanoscience Center (iNANO) and Department of Chemistry, Aarhus University, Langelandsgade 140, DK-8000 Aarhus C, Denmark

<sup>§</sup>Département de Chimie Physique, Sciences II, Université de Genève, 30, Quai Ernest-Ansermet, CH-1211 Genève 4, Switzerland

## S Supporting Information

**ABSTRACT:** Two reactive hydride composite systems,  $\text{Ca}(\text{BH}_4)_2\text{-NaNH}_2$  and  $\text{Mg}(\text{BH}_4)_2\text{-NaNH}_2$ , were systematically studied by in situ synchrotron radiation powder diffraction, in situ Fourier transform infrared spectroscopy, thermogravimetric analysis, and differential scanning calorimetry coupled with mass spectrometry. Metathesis reactions between the amides and borohydrides take place in both systems between 100 and 150 °C yielding amorphous materials with the proposed composition  $\text{M}(\text{BH}_4)(\text{NH}_2)$ . Simultaneously, a fraction of  $\text{NaNH}_2$  decomposes to  $\text{Na}_3\text{N}$  and ammonia via a complex pathway. The main gas released under 300 °C is ammonia for both systems, while significant amounts of hydrogen are released only above 350 °C.



## INTRODUCTION

In the past decade, the field of hydrogen storage has encountered a huge development due to the demand for cleaner and oil-independent transportation technologies. Light complex hydrides such as borohydrides, alanates, and amides have been intensively investigated as potential hydrogen storage materials, owing to their high gravimetric and volumetric hydrogen content.<sup>1</sup> Materials with high hydrogen content have been successfully designed, but a remaining challenge is to tune their dehydrogenation properties in order to deliver the contained hydrogen on demand. A promising approach for tailoring thermodynamic properties is to allow two or more hydrogen-containing materials to react with a release of hydrogen, forming different decomposition products than the pristine materials, thus tuning the enthalpy of the reaction.<sup>2</sup> Such hydride mixtures are denoted as reactive hydride composites (RHC). This approach has led to the discovery of reversible mixtures on the basis of otherwise nonreversible borohydrides,<sup>3–6</sup> as well as many hydrogen storage systems with improved properties including new complex bianionic or bimetallic hydrides.<sup>7–9</sup> Bianionic materials such as  $\text{Li}_4(\text{BH}_4)(\text{NH}_2)_3$  and  $\text{Mg}(\text{BH}_4)(\text{NH}_2)$  have also been investigated as ionic conductors.<sup>10–13</sup> As an example, it was shown that  $\text{LiBH}_4$  and  $\text{LiNH}_2$  form a complex bianionic compound  $\text{Li}_4(\text{BH}_4)(\text{NH}_2)_3$  releasing almost pure hydrogen above 250 °C (2–3 mol % of ammonia).<sup>14,15</sup> For comparison, pure  $\text{LiBH}_4$  releases hydrogen through a complex reaction scheme above 400 °C,<sup>1,16,17</sup> and  $\text{LiNH}_2$  releases ammonia upon thermal

decomposition through an acid–base disproportionation reaction:<sup>18</sup>



The lowered hydrogen release temperature of amide–borohydride systems may be ascribed to the interaction between partly positively charged hydrogen atoms of the amide anion with the partly negatively charged hydrogen atoms of the borohydride anion, as also observed for ammine metal borohydrides,  $\text{M}(\text{BH}_4)_m \cdot n\text{NH}_3$ .<sup>19–22</sup> Various amide–borohydride-based systems have been studied, such as  $\text{LiBH}_4\text{-LiNH}_2$ ,  $\text{NaBH}_4\text{-NaNH}_2$ ,  $\text{LiBH}_4\text{-Mg}(\text{NH}_2)_2$ , and  $\text{Mg}(\text{BH}_4)_2\text{-Mg}(\text{NH}_2)_2$ .<sup>9,10,23–33</sup> The only  $\text{NaNH}_2$ -based systems studied to date are  $\text{NaNH}_2\text{-NaBH}_4$  and very recently  $\text{NaNH}_2\text{-Ca}(\text{BH}_4)_2$  in 1:1 ratio.<sup>34</sup> However, this latter study was based mostly on TGA–DSC–MS data, and no in situ diffraction characterization was reported. Our present work can be seen as an extension of that study, including both in situ diffraction and in situ spectroscopy data, giving more emphasis on the transformations occurring to the samples during the heating process. The overall lower attention given to the  $\text{NaNH}_2$ -based systems compared to other hydrogen-rich systems might be due to the fact that sodium imide ( $\text{Na}_2\text{NH}$ ) does not form and that sodium nitride ( $\text{Na}_3\text{N}$ ) is known but unstable above 100 °C

Received: January 8, 2016

Revised: April 5, 2016

Published: April 6, 2016



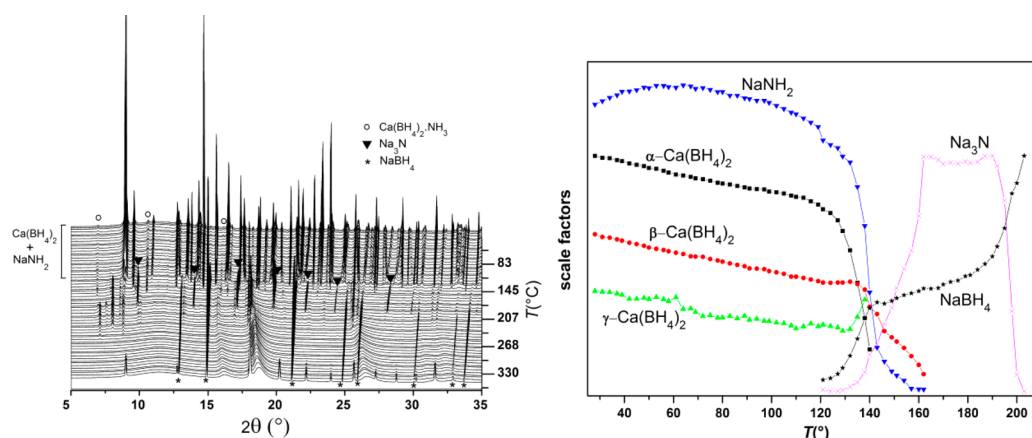


**Figure 1.** (a) In situ SR-PXD on CaNa12 heated from RT to 500 °C, 4 °C/min ( $\lambda = 0.819$  Å). (b) Scale factors from the sequential Rietveld refinement plotted versus temperature.

and is not straightforward to prepare,<sup>35–37</sup> thus limiting the possible reaction pathways.<sup>38</sup>

In this study, different mixtures of  $\text{Ca}(\text{BH}_4)_2$  or  $\text{Mg}(\text{BH}_4)_2$  with  $\text{NaNH}_2$  were investigated using in situ synchrotron radiation powder X-ray diffraction (PX), in situ Fourier transform infrared spectroscopy (FT-IR), and combined thermogravimetric analysis and differential scanning calorimetry coupled with mass spectrometry (TGA–DSC–MS).

## EXPERIMENTAL SECTION

**Sample Preparation.**  $\text{Ca}(\text{BH}_4)_2$  was synthesized by desorption of the commercially available  $\text{Ca}(\text{BH}_4)_2 \cdot 2\text{THF}$  complex (Aldrich) for 3 days at 160 °C under dynamic vacuum. The sample was analyzed by powder X-ray diffraction (PX) and showed to be a mixture of  $\alpha$ ,  $\beta$ , and  $\gamma$  polymorphs of  $\text{Ca}(\text{BH}_4)_2$ .  $\alpha$ - $\text{Mg}(\text{BH}_4)_2$  was obtained by desorption of the  $\text{Mg}(\text{BH}_4)_2 \cdot 1/2\text{Me}_2\text{S}$  complex synthesized by the solvent-mediated reaction between  $n\text{-Bu}_2\text{Mg}$  (Sigma-Aldrich, 1 M in heptane) and  $\text{Me}_2\text{S} \cdot \text{BH}_3$  (Sigma-Aldrich, 2 M in toluene).<sup>39</sup> PX showed only peaks corresponding to the unsolvated material. Commercial  $\text{NaNH}_2$  (Sigma-Aldrich; >90%) was used without purification.

$\text{Ca}(\text{BH}_4)_2$ – $\text{NaNH}_2$  samples were prepared by hand-grinding the powders in a mortar for 3 min in molar ratios 1:1, 1:2, and 1:3 and denoted CaNa11, CaNa12, and CaNa13, respectively. Upon grinding, the  $\text{Mg}(\text{BH}_4)_2$ – $\text{NaNH}_2$  mixtures undergo a reaction yielding mainly amorphous products. These samples were therefore prepared by gently mixing preground  $\text{Mg}(\text{BH}_4)_2$  and  $\text{NaNH}_2$  in order to avoid this amorphization reaction. Samples in ratios 1:1 and 1:2 were prepared, and they will be referred to as MgNa11 and MgNa12, respectively. All sample handling was performed in an argon-filled glovebox.

**Characterization.** *In-House Powder X-ray Diffraction (PX).* Measurements were performed using a MAR345 diffractometer. The X-ray source was a Rigaku ultraX18 molybdenum rotating anode equipped with a focusing mirror. The samples were packed under argon in glass capillaries of 0.5 mm outer diameter and sealed with wax.

*In Situ Synchrotron Radiation PX (SR-PX).* Measurements were conducted at the Swiss Norwegian Beamlines (SNBL) at the European Synchrotron Radiation Facility (ESRF) in Grenoble, France. The samples were mounted in glass capillaries sealed with wax. The wavelength was set to 0.82 Å, and the detector used was Pilatus 2M. Both in-house and

synchrotron two-dimensional diffraction images were integrated using the program Fit2D.<sup>40</sup> Calibration was performed using a standard lanthanum hexaboride sample.

**Temperature-Dependent Fourier Transform Infrared.** Experiments on solid samples were performed with a Biorad Excalibur Instrument equipped with a Specac Golden Gate heatable ATR setup. The spectral resolution was set to  $1\text{ cm}^{-1}$ . The samples were loaded in the Golden Gate inside the glovebox. The temperature was not linearly increased but manually set to a target temperature at which the measurement was performed before increasing the temperature to reach the next point.

**Thermal Analysis and Mass Spectrometry.** Thermogravimetric analysis (TGA) and differential scanning calorimetry (DSC) were made using a PerkinElmer STA 6000 apparatus simultaneously with mass spectrometry (MS) analysis of the residual gas with a Hiden Analytical HPR-20 QMS sampling system. The samples (approximately 5 mg) were placed in Al pans and heated from 40 to 500 °C (5 °C/min) under argon flow of 20 mL/min. The released gas was analyzed for hydrogen, ammonia, diborane, and nitrogen.

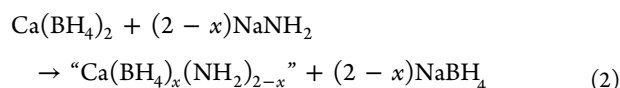
## RESULTS AND DISCUSSION

The behavior of these borohydride–amide systems is complex as many intermediates were observed during the in situ SR-PX measurements. It was necessary to combine the results of several characterization techniques and at different ratios to start having a picture of their reactivity. The main reaction scheme in the low- to mid-temperature range is the same in all the studied compositions. The case of  $\text{Ca}(\text{BH}_4)_2$ – $\text{NaNH}_2$  (1:2) is described at first in the next section as it was the key allowing understanding of the other related systems. Discussion of the other compositions will be done in comparison to this first one.

**In Situ SR-PX on  $\text{Ca}(\text{BH}_4)_2$ – $\text{NaNH}_2$ .** The in situ SR-PX data measured on  $\text{Ca}(\text{BH}_4)_2$ – $\text{NaNH}_2$  (1:2, CaNa12) between room temperature (RT) and 350 °C (4 °C/min) is presented in Figure 1a. The corresponding scale factors proportional to the amount of the crystalline phases exposed to the X-ray beam obtained by sequential Rietveld refinement are given in Figure 1b. The Rietveld refinement of the first pattern is available in the Supporting Information (Figure S2). At RT, Bragg diffraction is observed for the starting materials,  $\alpha$ -,  $\beta$ -, and  $\gamma$ - $\text{Ca}(\text{BH}_4)_2$  and  $\text{NaNH}_2$ , together with a very small amount of

$\text{Ca}(\text{BH}_4)_2 \cdot \text{NH}_3$  and  $\text{NaBH}_4$ . The scale factors for  $\text{Ca}(\text{BH}_4)_2 \cdot \text{NH}_3$  could not be calculated because the very low intensity of its reflections prevented it from being included in the sequential refinement. Between 120 and 130 °C, the peaks of the starting materials begin to decrease in intensity while the reflections of  $\text{Ca}(\text{BH}_4)_2 \cdot \text{NH}_3$  start to increase. Upon further heating, the starting materials disappear at 160 °C. In the early stages of this reaction,  $\text{NaBH}_4$  is formed. Its diffraction intensity reaches a plateau at 140 °C; the slow but constant subsequent increase may be attributed to an increase of the crystallinity. Between 140 and 160 °C,  $\text{Na}_3\text{N}$  is the main forming compound (Figure 1b). The growth of its fraction stops with the complete disappearance of the starting materials. Above 190 °C,  $\text{Na}_3\text{N}$  disappears from the diffraction pattern. This decrease is accompanied by an increase of  $\text{NaBH}_4$  peaks. Several unknown crystalline compounds as well as amorphous material(s) whose presence is indicated by wide humps are observed in the temperature range of 150–250 °C. Above 250 °C,  $\text{NaBH}_4$  is the only observed crystalline compound. The new peaks appearing above 330 °C likely correspond to a material formed by a reaction with the walls of the capillary and ambient air as the powder and capillary were fused together at this stage.

These observations suggest that two reactions occur in parallel above 130 °C, the first one being a metathesis between the starting compounds, yielding  $\text{NaBH}_4$  and an amorphous mixed-anion calcium amide borohydride,  $\text{Ca}(\text{BH}_4)_x(\text{NH}_2)_{2-x}$  (reaction 2). The second reaction is the decomposition of  $\text{NaNH}_2$  into  $\text{Na}_3\text{N}$  with a release of ammonia (reaction 3). The formation of ammonia explains the appearance of  $\text{Ca}(\text{BH}_4)_2 \cdot \text{NH}_3$ . The observation of this latter compound after grinding the sample at room temperature can only be explained by the release of ammonia by  $\text{NaNH}_2$ . The fact that a small amount of  $\text{NaBH}_4$  is also observed supports the idea of a mechanism similar to the one occurring at 130 °C. This was not further investigated because the amounts of  $\text{NaBH}_4$  and  $\text{Ca}(\text{BH}_4)_2 \cdot \text{NH}_3$  at RT are very small.



It is worth noting that the formation of  $\text{Na}_3\text{N}$  is not observed either in the thermal decomposition of pure sodium amide (Figure S1 in the Supporting Information) or in the decomposition of  $\text{NaNH}_2$ – $\text{NaBH}_4$  mixtures.<sup>23,29</sup> Reaction 3 is therefore a simplified view of a more complex reaction scheme likely involving calcium-containing species. It should also be noted that  $\text{Na}_3\text{N}$  was reported to decompose into nitrogen and metallic sodium at around 100 °C in an internal redox reaction.<sup>35,36</sup> In our case, it is formed above its reported decomposition temperature, which may be due to an increased partial pressure of  $\text{NH}_3$  in the closed capillary. Furthermore, it does not decompose into elements but seems to further react forming  $\text{NaBH}_4$ . Considering that the oxidation state of sodium remains unchanged in this latter transformation, the byproduct likely contains nitrogen in the same oxidation state as in the amide and nitride anions (-III); thus, the product is a calcium nitride related compound. The formation of  $\text{NaBH}_4$  at this stage requires the presence of  $\text{BH}_4$  anions and therefore supports the hypothesis of the presence of amorphous  $\text{Ca}(\text{BH}_4)_x(\text{NH}_2)_{2-x}$ . Alternatively, the compounds may form a eutectic liquid out of which  $\text{NaBH}_4$  would crystallize;<sup>41</sup> this

was however rejected after visually checking the heating process of the CaNa12 sample in a glass tube.

The results of the in situ SR-PXD on  $\text{Ca}(\text{BH}_4)_2$ – $\text{NaNH}_2$  (1:1), (1:2), and (1:3) are summarized in Table 1, and the in

**Table 1. Compounds Observed by in Situ SR–PXD at Different Temperatures**

| compound                                     | temperature domain where the compound is observed (°C) |         |              |
|--|--|---------|--------------|
|  | CaNa11   | CaNa12  | CaNa13       |
| $\alpha$ - $\text{Ca}(\text{BH}_4)_2$        | 25–160   | 25–150  | 25–145       |
| $\beta$ - $\text{Ca}(\text{BH}_4)_2$         | 25–190   | 25–160  | 25–150       |
| $\gamma$ - $\text{Ca}(\text{BH}_4)_2$        | 25–170   | 25–150  | 25–145       |
| $\text{NaNH}_2$                              | 25–145   | 25–150  | 25–165       |
| $\text{Ca}(\text{BH}_4)_2 \cdot \text{NH}_3$ | 130–165  | 25–170  | 25–170       |
| $\text{Na}_3\text{N}$                        | 150–190  | 140–200 | 135–185      |
| $\text{NaBH}_4$                              | 180–end  | 130–330 | not observed |
| unknown                                      | 180–end  | 130–245 | 135–220      |

situ SR-PXD plots for CaNa11 and CaNa13 samples are presented in Figures S3 and S4. The similarity between these results shows that the main reaction pathway is identical in all samples. In the 1:1 ratio,  $\text{Ca}(\text{BH}_4)_2$  is observed up to 190 °C, 45 °C higher than  $\text{NaNH}_2$ , whereas for the 1:3 ratio,  $\text{NaNH}_2$  is observed up to higher temperatures than  $\text{Ca}(\text{BH}_4)_2$ . For the 1:2 ratio, they disappear from the diffraction pattern at a similar temperature, showing that the reaction occurring at this point has a ratio close to 1:2. The fact that  $\text{NaBH}_4$  is not observed in the 1:3 ratio cannot be explained either by the metathesis reaction or by the decomposition of  $\text{NaNH}_2$  in  $\text{Na}_3\text{N}$ . The lack of  $\text{BH}_4$  anions to form  $\text{NaBH}_4$  could only be explained by a reaction consuming the  $\text{BH}_4$  anion in excess of  $\text{NaNH}_2$ .

**In Situ FT-IR on  $\text{Ca}(\text{BH}_4)_2$ – $\text{NaNH}_2$  (1:2).** The in situ IR measurement (Figure 2) between RT and 280 °C complements the diffraction data, giving more insight into the fate of the  $\text{BH}_4$  and  $\text{NH}_2$  anions. The most relevant details of this study are the B–H bending region between 1000 and 1500  $\text{cm}^{-1}$  and the N–H stretching region around 3300  $\text{cm}^{-1}$  where the  $\text{NH}_2$  anion gives typical symmetric and asymmetric stretching peaks. Expansions of these regions are given in the Supporting Information as well as the N–H stretching region of pure  $\text{NaNH}_2$  for comparison (Figures S5–S7).

At RT, the absorption patterns are consistent with a mixture of  $\text{Ca}(\text{BH}_4)_2$  and  $\text{NaNH}_2$ . The spectra remain unchanged up to 150 °C, where a modification in the peak shapes for the  $\text{BH}_4$  and  $\text{NH}_2$  bands occurs, corresponding to the disappearance of the starting materials observed by in situ SR-PXD. While the N–H stretching peaks at 3211 and 3259  $\text{cm}^{-1}$  disappear, two new peaks appear at slightly higher wavenumbers (3235 and 3285  $\text{cm}^{-1}$ ) showing that the  $\text{NH}_2$  anion does not fully decompose into  $\text{Na}_3\text{N}$  during the reaction occurring around 150 °C. These two new peaks are consistent with the symmetric and asymmetric stretching modes of a new  $[\text{NH}_2]^-$ -containing material, however invisible in the diffraction experiment. The N–H bending mode, visible at around 1550  $\text{cm}^{-1}$ , supports this hypothesis as the peak is slightly blue-shifted, but still present until 250 °C just as the stretching peaks. These shifted positions do not correspond to  $\text{Ca}(\text{NH}_2)_2$  for which the IR spectrum is known.<sup>42</sup>

In the B–H bending region, the typical  $\text{Ca}(\text{BH}_4)_2$  absorption band fades into another pattern with bands centered at 1105, 1180, and 1215  $\text{cm}^{-1}$ . The first of these bands corresponds to

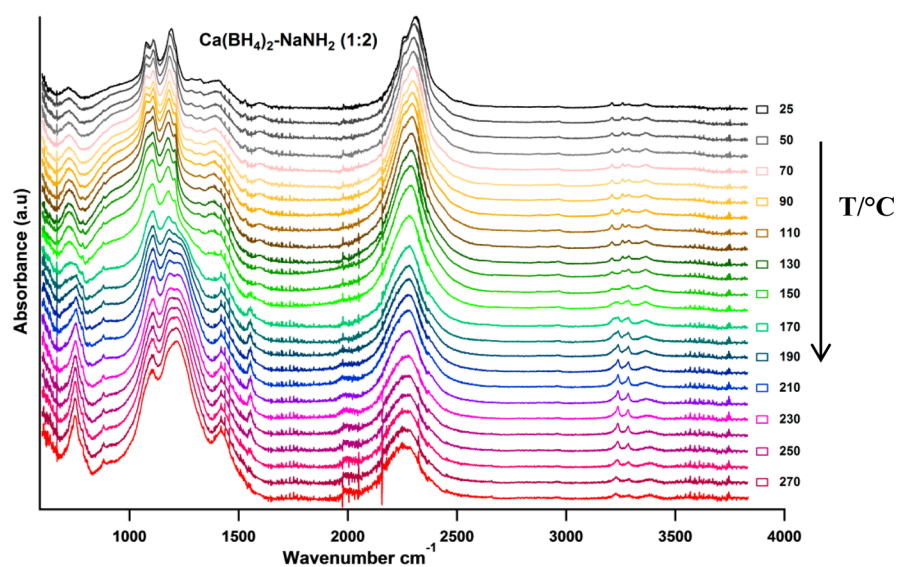


Figure 2. In situ FT-IR of CaNa12 heated in steps of 10 °C from RT to 280 °C.

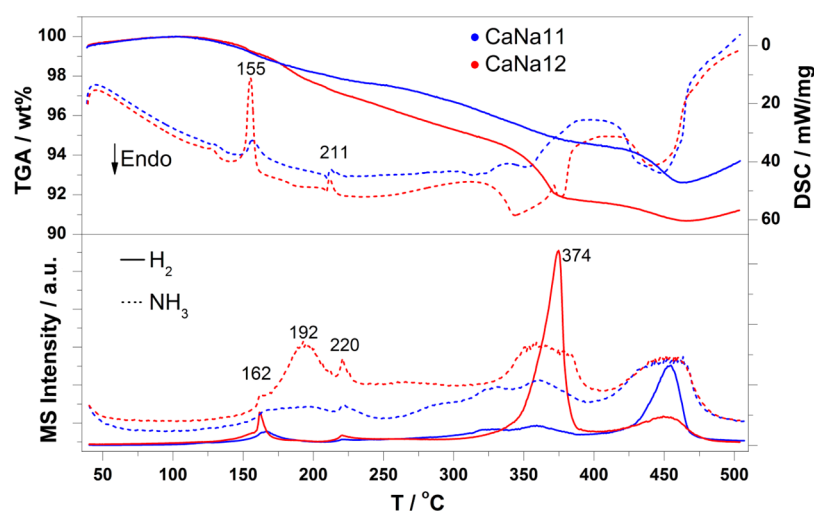


Figure 3. Top: TGA (line) and DSC (dashed) for CaNa11 (blue) and CaNa12 (red) heated from RT to 500 °C (5 °C/min) in argon atmosphere. Bottom: Related MS signals for hydrogen (line) and ammonia (dashed).

$\text{NaBH}_4$ <sup>43,44</sup> in accord with the X-ray experiment. However,  $\text{NaBH}_4$  does not contribute to the bands centered at 1180 and 1215  $\text{cm}^{-1}$ , which shows that there are B–H bonds with a different environment than in  $\text{NaBH}_4$ . These observations confirm that the reaction observed at 150 °C is an exchange reaction between  $\text{NaNH}_2$  and  $\text{Ca}(\text{BH}_4)_2$  forming some  $\text{Ca}(\text{NH}_2)_x(\text{BH}_4)_{2-x}$ -type compound. No further changes are observed in the B–H bending region when the N–H vibration modes disappear above 250 °C.

**Thermal Analysis of  $\text{Ca}(\text{BH}_4)_2$ – $\text{NaNH}_2$  in 1:1 and 1:2 Ratios.** Combined thermogravimetric analysis (TGA) and differential scanning calorimetry (DSC) coupled to a mass spectrometer (MS) were performed for CaNa11 and CaNa12 from RT to 500 °C (5 °C/min); see Figure 3. The onset temperature for gas release is 125 °C for both samples, and there is a nonlinear but continuous mass loss up to 450 °C of about 7.5 and 9 wt %, respectively. The DSC curves show three exothermic peaks in the region 100–250 °C out of which the second one (155 °C) is the most intense, especially for the CaNa12 sample. These peaks do not correlate with the gas

release steps. Above 300 °C, the DSC signal becomes complex and was not analyzed in detail.

The first slightly exothermic peak at 130 °C can be assigned to the exchange reaction 2 between the starting materials described in the sections above. The second peak (155 °C) can be related to the formation of  $\text{Na}_3\text{N}$  observed in the diffraction experiment, occurring mainly between 150 and 160 °C; see reaction 3. The assignment of the peak at 211 °C is however not straightforward.  $\text{Na}_3\text{N}$  disappears from the diffraction patterns between 190 and 200 °C. Such a discrepancy is not huge considering that the sample environment is different in both experiments, but still surprising considering the fact that the previous events occur at a very close temperature.

The analysis of desorbed gases by mass spectrometry (Figure 3, bottom) shows that mainly ammonia is released in several steps below 300 °C. The first step peaks at 162 °C and involves the release of a small amount of hydrogen. The second step is a pure ammonia release reaching its maximum at 192 °C. This step is more pronounced for sample CaNa12 than for CaNa11 which shows that it may be due to a reaction of the amide group without any change on the borohydride part. The third

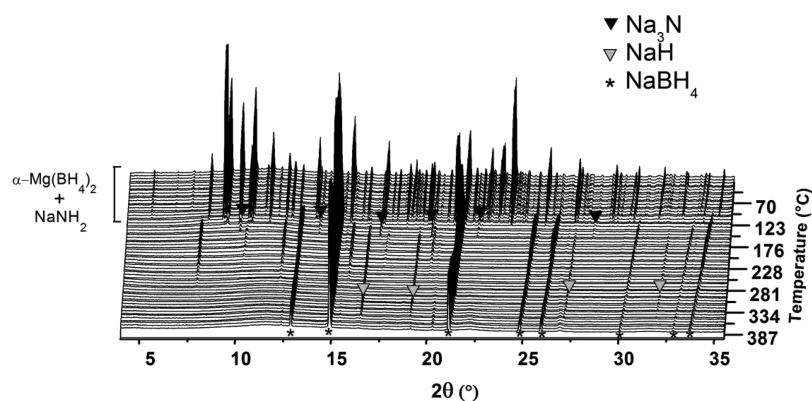


Figure 4. In situ SR-PXD on sample MgNa11 (RT  $\rightarrow$  500 °C, 4 °C/min,  $\lambda$  = 0.819 Å).

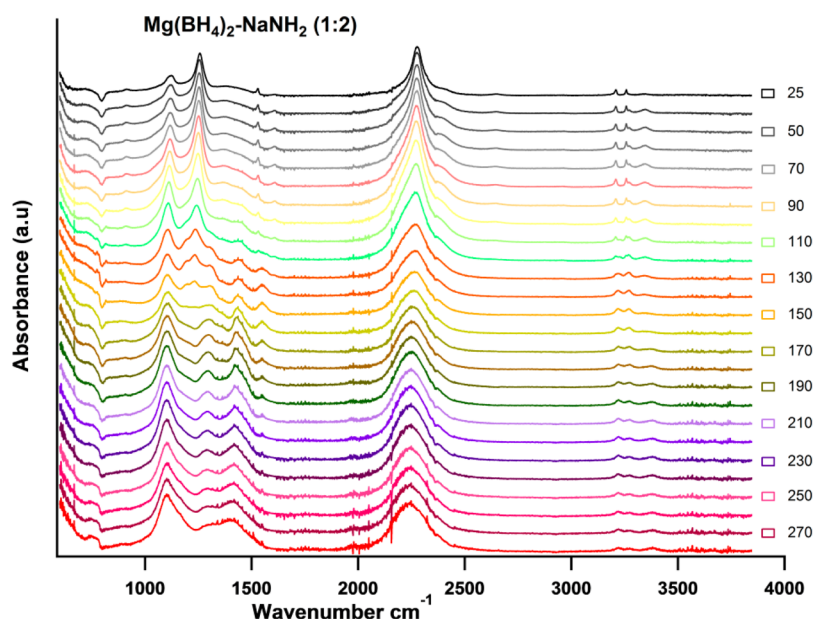


Figure 5. In situ FT-IR of MgNa12 heated from room temperature to 280 °C in steps of 10 °C.

step is a release of ammonia and of a small amount of hydrogen at 220 °C. From RT to 250 °C, the behaviors of both samples are quite similar. The main hydrogen release peaks occur above 350 °C for both samples and are correlated with ammonia release and broad endothermic bands. It is observed that the main hydrogen release occurs at a lower temperature when the amount of amide is higher, showing the destabilization effect of protic hydrogens on the  $\text{BH}_4$  anion.

**In Situ SR-PXD on  $\text{Mg}(\text{BH}_4)_2\text{-NaNH}_2$ .** The behavior of the  $\text{Mg}(\text{BH}_4)_2\text{-NaNH}_2$  system is similar to that of the  $\text{Ca}(\text{BH}_4)_2\text{-NaNH}_2$  system. As shown for the MgNa11 sample in Figure 4, the starting materials disappear from the diffraction pattern slightly above 100 °C, and sodium nitride ( $\text{Na}_3\text{N}$ ) and sodium borohydride ( $\text{NaBH}_4$ ) form. After this event, the only observed crystalline compounds are  $\text{NaBH}_4$ , which is by far dominating the diffraction pattern, a small amount of  $\text{NaH}$ , and another unknown compound. No known magnesium-containing compounds are observed. No significant difference was observed between the MgNa11 and MgNa12 samples (Figure S8).

**In Situ IR on  $\text{Mg}(\text{BH}_4)_2\text{-NaNH}_2$ .** As shown in Figure 5, the behavior of the MgNa12 sample is similar to the one of CaNa12 presented above. The N–H stretching peaks between

3150 and 3400  $\text{cm}^{-1}$  remain throughout the experiment although their shape and the exact position change. However, the N–H bending peak seems to disappear between 190 and 210 °C indicating that the nitrogen-containing species above this temperature is an imide ( $[\text{NH}]^{2-}$ ) and not an amide. The B–H bending band undergoes a first modification between 110 and 130 °C, a second between 150 and 170 °C, and a third at higher temperatures. During the first event, the characteristic bands of  $\text{Mg}(\text{BH}_4)_2$  at 1125 and 1253  $\text{cm}^{-1}$  disappear while new bands appear at 1105  $\text{cm}^{-1}$  ( $\text{NaBH}_4$ ), 1190, and 1310  $\text{cm}^{-1}$ . This event can be attributed to the proposed metathesis reaction between the starting materials forming  $\text{NaBH}_4$  and “ $\text{Mg}(\text{BH}_4)_{2-x}(\text{NH}_2)_x$ ” as observed in the in situ-PXD experiment and in the same way as in the calcium-based system. It is worth noting that the reported compound  $\text{Mg}(\text{BH}_4)(\text{NH}_2)$  was not observed in the X-ray diffraction experiment and that its IR spectrum is unfortunately unknown.<sup>45</sup> Most likely, the crystalline  $\text{Mg}(\text{BH}_4)(\text{NH}_2)$  forms only after extended annealing, and its crystallization is missed in our variable temperature experiments. During the second event, the peaks at 1190 and 1310  $\text{cm}^{-1}$  disappear and two new peaks appear at 1295 and 1430  $\text{cm}^{-1}$ . This coincides with the appearance of a broad peak at 1550  $\text{cm}^{-1}$  in the N–H bending region, slightly blue-shifted

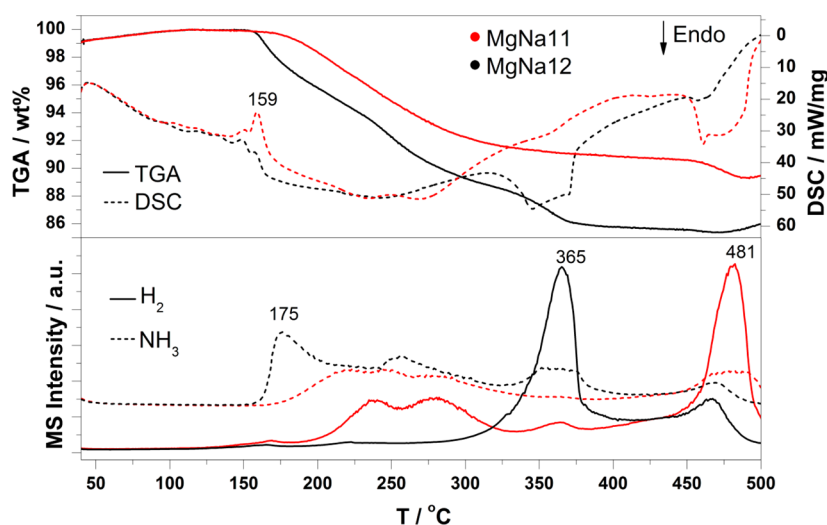


**Figure 6.** Top: TGA (line) and DSC (dashed) for MgNa11 (red) and MgNa12 (black) heated from RT to 500 °C (5 °C/min) in argon atmosphere. Bottom: Related MS signals for hydrogen (line) and ammonia (dashed).

compared with the original bending mode of  $\text{NaNH}_2$  indicating a structural rearrangement in the amorphous " $\text{Mg}(\text{BH}_4)_{2-x}(\text{NH}_2)_x$ ". The third and last event is the progressive disappearance of the B–H bending peaks at 1295 and 1430  $\text{cm}^{-1}$  together with the broad peak from the N–H bending region. The fact that these peaks appear and disappear together is a hint that they belong to the same material, reinforcing the hypothesis of the existence of an amorphous  $\text{Mg}(\text{BH}_4)_{2-x}(\text{NH}_2)_x$  type of material.

**Thermal Analysis of  $\text{Mg}(\text{BH}_4)_2\text{--NaNH}_2$ .** The TGA and DSC curves associated with the MS signals for MgNa11 and MgNa12 are shown in Figure 6. The desorption starts at 175 and 158 °C for the MgNa11 and MgNa12 samples, respectively, with total mass losses of 10.7 and 14.7 wt %. Similarly to the that of calcium-based system, the mass loss does not occur in clear steps but is rather continuous, though nonlinear. Few exothermic events are observed for both samples between 100 and 160 °C, before the desorption starts. They can be related to the metathesis reaction occurring in this temperature range. At higher temperature, endothermic bands are observed between 450 and 490 °C for MgNa11 and between 330 and 375 °C for MgNa12. These endothermic events correspond to a faster mass loss in the TGA curve and to the main hydrogen release peaks as seen in the MS signal.

The high mass losses observed prove that not only hydrogen is released upon thermal decomposition, as they exceed the total hydrogen content of the samples. Making the assumption that there is no hydrogen left in the sample at 500 °C and that the only desorbed gases are  $\text{NH}_3$  and  $\text{H}_2$ , it can be easily calculated that the measured 14.7 wt % desorption for MgNa12 corresponds to a desorption of 0.53 and 5.21 mol of ammonia and hydrogen. In other words, there is an average of 9.2 mol % of ammonia in the released gas over the desorption process. This value is likely underestimated as the sample might still contain some hydrogen-containing compounds. Furthermore, the MS signal shows that most of the ammonia is released at much lower temperature than hydrogen.

## CONCLUSION

The two newly investigated hydrogen-rich systems,  $\text{Ca}(\text{BH}_4)_2\text{--NaNH}_2$  and  $\text{Mg}(\text{BH}_4)_2\text{--NaNH}_2$ , undergo a metathesis reaction yielding amorphous materials and  $\text{NaBH}_4$  between

100 and 150 °C. In parallel to this reaction, part of the sodium amide decomposes into sodium nitride with a release of ammonia via a complex reaction scheme. The gas release occurs in several steps over a broad temperature range. Despite a relatively low onset temperature for gas release of ca. 150 °C for all samples, the main hydrogen desorption peaks occur only at 374 and 365 °C in the calcium-based and magnesium-based systems with 1:2 ratio, respectively. In the 1:1 ratio, the main hydrogen release peaks occur at even higher temperatures: 481 °C for the magnesium-based system and 460 °C for the calcium-based system. The lowered temperature of hydrogen desorption with higher amount of amide supports the idea of the destabilization of borohydrides by amides. However, the complexity of the reaction pathways in these systems, the release of ammonia, and the lowered but still high temperature of the main hydrogen desorption event make them impractical for hydrogen storage applications. More interesting is the formation of  $\text{Na}_3\text{N}$  resulting from the destabilization of  $\text{NaNH}_2$  by  $\text{Ca}(\text{BH}_4)_2$  and to a smaller extend by  $\text{Mg}(\text{BH}_4)_2$  observed for the first time in this study as it might open a new route for the synthesis of sodium nitride.

## ASSOCIATED CONTENT

### Supporting Information

The Supporting Information is available free of charge on the ACS Publications website at DOI: 10.1021/acs.jpcc.6b00209.

In situ SR-PXD plots for various samples; zooms on the regions in the in situ FT-IR data, FT-IR, and SR-PXD of pure  $\text{NaNH}_2$  (PDF)

## AUTHOR INFORMATION

### Corresponding Author

\*E-mail: yaroslav.flinchuk@uclouvain.be. Fax: +32-10-47-27-07.

### Notes

The authors declare no competing financial interest.

## ACKNOWLEDGMENTS

The authors gratefully acknowledge the Belgian *Fonds National pour la recherche Scientifique* (FNRS) and *Fonds pour la Formation à la recherche en Industrie et en Agriculture* (FRIA) for

funding. The authors acknowledge the ESRF for the beamtime allocation and the staff of the Swiss-Norwegian Beamlines where the in situ SR-PXD experiments were conducted. Part of this work was supported by the Danish National Research Foundation, Center for Materials Crystallography (DNRF93), the Innovation Fund Denmark (project HyFill-Fast), and the Danish Research Council for Nature and Universe (Danscatt). This work was supported in part by the Swiss National Science Foundation.

## REFERENCES

- (1) Rude, L. H.; Nielsen, T. K.; Ravnsbæk, D. B.; Bösenberg, V.; Ley, M. B.; Richter, B.; Arnbjerg, L. M.; Dornheim, M.; Filinchuk, Y.; Besenbacher, F.; et al. Tailoring Properties of Borohydrides for Hydrogen Storage: A Review. *Phys. Status Solidi A* **2011**, *208*, 1754–1773.
- (2) Jepsen, L. H.; Ley, M. B.; Lee, Y.-S.; Cho, Y. W.; Dornheim, M.; Jensen, J. O.; Filinchuk, Y.; Jørgensen, J. E.; Besenbacher, F.; Jensen, T. R. Boron–Nitrogen Based Hydrides and Reactive Composites for Hydrogen Storage. *Mater. Today* **2014**, *17*, 129–135.
- (3) Barkhordarian, G.; Klassen, T.; Dornheim, M.; Bormann, R. Unexpected Kinetic Effect of  $\text{MgB}_2$  in Reactive Hydride Composites Containing Complex Hydrides. *J. Alloys Compd.* **2007**, *440*, 18–21.
- (4) Chen, P.; Xiong, Z.; Luo, J.; Lin, J.; Tan, K. L. Interaction of Hydrogen with Metal Nitrides and Imides. *Nature* **2002**, *420*, 302–304.
- (5) Luo, W.; Sickafoose, S. Thermodynamic and Structural Characterization of the Mg–Li–N–H Hydrogen Storage System. *J. Alloys Compd.* **2006**, *407*, 274–281.
- (6) Vajo, J. J.; Skeith, S. L.; Mertens, F. Reversible Storage of Hydrogen in Destabilized  $\text{LiBH}_4$ . *J. Phys. Chem. B* **2005**, *109*, 3719–3722.
- (7) Schouwink, P.; D’Anna, V.; Ley, M. B.; Lawson Daku, L. M.; Richter, B.; Jensen, T. R.; Hagemann, H.; Černý, R. Bimetallic Borohydrides in the System  $\text{M}(\text{BH}_4)_2\text{–KBH}_4$  ( $\text{M} = \text{Mg}, \text{Mn}$ ): on the Structural Diversity. *J. Phys. Chem. C* **2012**, *116*, 10829–10840.
- (8) Ley, M. B.; Ravnsbæk, D. B.; Filinchuk, Y.; Lee, Y.-S.; Janot, R.; Cho, Y. W.; Skibsted, J.; Jensen, T. R.  $\text{LiCe}(\text{BH}_4)_3\text{Cl}$ , a New Lithium-Ion Conductor and Hydrogen Storage Material with Isolated Tetranuclear Anionic Clusters. *Chem. Mater.* **2012**, *24*, 1654–1663.
- (9) Ravnsbæk, D. B.; Sørensen, L. H.; Filinchuk, Y.; Besenbacher, F.; Jensen, T. R. Screening of Metal Borohydrides by Mechanochemistry and Diffraction. *Angew. Chem., Int. Ed.* **2012**, *51*, 3582–3586.
- (10) Matsuo, M.; Remhof, A.; Martelli, P.; Caputo, R.; Ernst, M.; Miura, Y.; Sato, T.; Oguchi, H.; Maekawa, H.; Takamura, H.; et al. Complex Hydrides with  $(\text{BH}_4)^-$  and  $(\text{NH}_2)^-$  Anions as New Lithium Fast-Ion Conductors. *J. Am. Chem. Soc.* **2009**, *131*, 16389–16391.
- (11) Ley, M. B.; Jepsen, L. H.; Lee, Y.-S.; Cho, Y. W.; Bellosta Von Colbe, J. M.; Dornheim, M.; Rokni, M.; Jensen, J. O.; Sloth, M.; Filinchuk, Y.; et al. Complex Hydrides for Hydrogen Storage—New Perspectives. *Mater. Today* **2014**, *17*, 122–128.
- (12) Remhof, A.; Yan, Y.; Embs, J. P.; Sakai, V. G.; Nale, A.; de Jongh, P.; Lodzińska, Z.; Züttel, A. Rotational Disorder in Lithium Borohydride. *EPJ Web Conf.* **2015**, *83*, 02014.
- (13) Higashi, S.; Miwa, K.; Aoki, M.; Takechi, K. A Novel Inorganic Solid State Ion Conductor for Rechargeable Mg Batteries. *Chem. Commun.* **2014**, *50*, 1320–1322.
- (14) Pinkerton, F. E.; Meisner, G. P.; Meyer, M. S.; Balogh, M. P.; Kundrat, M. D. Hydrogen Desorption Exceeding Ten Weight Percent from the New Quaternary Hydride  $\text{Li}_3\text{BN}_2\text{H}_8$ . *J. Phys. Chem. B* **2005**, *109*, 6–8.
- (15) Filinchuk, Y.; Yvon, K.; Meisner, G. P.; Pinkerton, F. E.; Balogh, M. P. On the Composition and Crystal Structure of the New Quaternary Hydride Phase  $\text{Li}_4\text{BN}_3\text{H}_{10}$ . *Inorg. Chem.* **2006**, *45*, 1433–1435.
- (16) Mosegaard, L.; Møller, B.; Jørgensen, J. E.; Bösenberg, U.; Dornheim, M.; Hanson, J. C.; Cerenius, Y.; Walker, G.; Jakobsen, H. J.; Besenbacher, F.; et al. Intermediate Phases Observed During Decomposition of  $\text{LiBH}_4$ . *J. Alloys Compd.* **2007**, *446–447*, 301–305.
- (17) Pitt, M. P.; Paskevicius, M.; Brown, D. H.; Sheppard, D. A.; Buckley, C. E. Thermal Stability of  $\text{Li}_2\text{B}_{12}\text{H}_{12}$  and Its Role in the Decomposition of  $\text{LiBH}_4$ . *J. Am. Chem. Soc.* **2013**, *135*, 6930–694.
- (18) Ichikawa, T.; Isobe, S.; Hanada, N.; Fujii, H. Lithium Nitride for Reversible Hydrogen Storage. *J. Alloys Compd.* **2004**, *365*, 271–276.
- (19) Jepsen, L. H.; Ley, M. B.; Černý, R.; Lee, Y.-S.; Cho, Y. W.; Ravnsbæk, D.; Besenbacher, F.; Skibsted, J.; Jensen, T. R. Trends in Syntheses, Structures, and Properties for Three Series of Ammine Rare-Earth Metal Borohydrides,  $\text{M}(\text{BH}_4)_3\cdot n\text{NH}_3$  ( $\text{M} = \text{Y}, \text{Gd}$ , and Dy). *Inorg. Chem.* **2015**, *54*, 7402–7414.
- (20) Jepsen, L. H.; Ley, M. B.; Filinchuk, Y.; Besenbacher, F.; Jensen, T. R. Tailoring the Properties of Ammine Metal Borohydrides for Solid-State Hydrogen Storage. *ChemSusChem* **2015**, *8*, 1452–1463.
- (21) Soloveichik, G.; Her, J.-H.; Stephens, P. W.; Gao, Y.; Rijssenbeek, J.; Andrus, M.; Zhao, J.-C. Ammine Magnesium Borohydride Complex as a New Material for Hydrogen Storage: Structure and Properties of  $\text{Mg}(\text{BH}_4)_2\cdot 2\text{NH}_3$ . *Inorg. Chem.* **2008**, *47*, 4290–4298.
- (22) Chu, H.; Wu, G.; Xiong, Z.; Guo, J.; He, T.; Chen, P. Structure and Hydrogen Storage Properties of Calcium Borohydride Diammoniate. *Chem. Mater.* **2010**, *22*, 6021–6028.
- (23) Wu, C.; Bai, Y.; Yang, J.; Wu, F.; Long, F. Characterizations of Composite  $\text{NaNH}_2\text{–NaBH}_4$  Hydrogen Storage Materials Synthesized via Ball Milling. *Int. J. Hydrogen Energy* **2012**, *37*, 889–893.
- (24) Noritake, T.; Aoki, M.; Towata, S.; Ninomiya, A.; Nakamori, Y.; Orimo, S. Crystal Structure Analysis of Novel Complex Hydrides Formed by the Combination of  $\text{LiBH}_4$  and  $\text{LiNH}_2$ . *Appl. Phys. A: Mater. Sci. Process.* **2006**, *83*, 277–279.
- (25) Chen, X. Y.; Guo, Y. H.; Yu, X. B. Enhanced Dehydrogenation Properties of Modified  $\text{Mg}(\text{NH}_2)_2\text{–LiBH}_4$  Composites. *J. Phys. Chem. C* **2010**, *114*, 17947–17953.
- (26) Chu, H.; Wu, G.; Zhang, Y.; Xiong, Z.; Guo, J.; He, T.; Chen, P. Improved Dehydrogenation Properties of Calcium Borohydride Combined with Alkaline-Earth Metal Amides. *J. Phys. Chem. C* **2011**, *115*, 18035–18041.
- (27) Yu, X. B.; Yang, Z. X.; Guo, Y. H.; Li, S. G. Thermal Decomposition Performance of  $\text{Ca}(\text{BH}_4)_2/\text{LiNH}_2$  Mixtures. *J. Alloys Compd.* **2011**, *509*, S724–S727.
- (28) Somer, M.; Acar, S.; Koz, C.; Kokal, I.; Höhn, P.; Cardoso-Gil, R.; Aydemir, U.; Akselrud, L.  $\alpha$ - and  $\beta$ - $\text{Na}_2[\text{BH}_4][\text{NH}_2]$ : Two Modifications of a Complex Hydride in the System  $\text{NaNH}_2\text{–NaBH}_4$ ; Syntheses, Crystal Structures, Thermal Analyses, Mass and Vibrational Spectra. *J. Alloys Compd.* **2010**, *491*, 98–105.
- (29) Zhang, Y.; Tian, Q. The Reactions in  $\text{LiBH}_4\text{–NaNH}_2$  Hydrogen Storage System. *Int. J. Hydrogen Energy* **2011**, *36*, 9733–9742.
- (30) Chater, P. A.; David, W. I. F.; Anderson, P. A. Synthesis and Structure of the New Complex Hydride  $\text{Li}_2\text{BH}_4\text{NH}_2$ . *Chem. Commun.* **2007**, *45*, 4770–4772.
- (31) Chater, P. A.; Anderson, P. A.; Prendergast, J. W.; Walton, A.; Mann, V. S. J.; Book, D.; David, W. I. F.; Johnson, S. R.; Edwards, P. P. Synthesis and Characterization of Amide–Borohydrides: New Complex Light Hydrides for Potential Hydrogen Storage. *J. Alloys Compd.* **2007**, *446–447*, 350–354.
- (32) Chu, H.; Xiong, Z.; Wu, G.; Guo, J.; Zheng, X.; He, T.; Wu, C.; Chen, P. Hydrogen Storage Properties of  $\text{Ca}(\text{BH}_4)_2\text{–LiNH}_2$  System. *Chem. - Asian J.* **2010**, *5*, 1594–1599.
- (33) Chu, H.; Xiong, Z.; Wu, G.; Guo, J.; He, T.; Chen, P. Improved Dehydrogenation Properties of  $\text{Ca}(\text{BH}_4)_2\text{–LiNH}_2$  Combined System. *Dalton Trans.* **2010**, *39*, 10585–10587.
- (34) Poonyayant, N.; Stavila, V.; Majzoub, E. H.; Klebanoff, L. E.; Behrens, R.; Angboonpong, N.; Ulutagay-Kartin, M.; Pakawatpanurut, P.; Hecht, E. S.; Breit, J. S. An Investigation into the Hydrogen Storage Characteristics of  $\text{Ca}(\text{BH}_4)_2/\text{LiNH}_2$  and  $\text{Ca}(\text{BH}_4)_2/\text{NaNH}_2$ : Evidence of Intramolecular Destabilization. *J. Phys. Chem. C* **2014**, *118*, 14759–14769.
- (35) Fischer, D.; Jansen, M. Synthesis and Structure of  $\text{Na}_3\text{N}$ . *Angew. Chem., Int. Ed.* **2002**, *41*, 1755–1756.

- (36) Vajenine, G. V. Plasma-Assisted Synthesis and Properties of  $\text{Na}_3\text{N}$ . *Inorg. Chem.* **2007**, *46*, 5146–5148.
- (37) Niewa, R.  $\text{Na}_3\text{N}$  - An Original Synthetic Route for a Long Sought After Binary Nitride. *Angew. Chem., Int. Ed.* **2002**, *41*, 1701–1702.
- (38) Sheppard, D. A.; Paskevicius, M.; Buckley, C. E. Hydrogen Desorption from the  $\text{NaNH}_2\text{-MgH}_2$  System. *J. Phys. Chem. C* **2011**, *115*, 8407–8413.
- (39) Zanella, P.; Crociani, L.; Masciocchi, N.; Giunchi, G. Facile High-Yield Synthesis of Pure, Crystalline  $\text{Mg}(\text{BH}_4)_2$ . *Inorg. Chem.* **2007**, *46*, 9039–9041.
- (40) Hammersley, A. P. Fit 2D: AN Introduction and Overview. *ESRF Internal Report*, 1997, ESRF97HA02T.
- (41) Paskevicius, M.; Ley, M. B.; Sheppard, D. A.; Jensen, T. R.; Buckley, C. E. Eutectic Melting in Metal Borohydrides. *Phys. Chem. Chem. Phys.* **2013**, *15*, 19774–19789.
- (42) Linde, G.; Juza, R. IR-Spektren von Amiden und Imiden zwei- und dreiwertiger Metalle. *Z. Anorg. Allg. Chem.* **1974**, *409*, 199–214.
- (43) D'Anna, V.; Spyratou, A.; Sharma, M.; Hagemann, H. FT-IR Spectra of Inorganic Borohydrides. *Spectrochim. Acta, Part A* **2014**, *128*, 902–906.
- (44) Renaudin, G.; Gomes, S.; Hagemann, H.; Keller, L.; Yvon, K. Structural and Spectroscopic Studies on the Alkali Borohydrides  $\text{MBH}_4$  ( $M = \text{Na, K, Rb, Cs}$ ). *J. Alloys Compd.* **2004**, *375*, 98–106.
- (45) Noritake, T.; Miwa, K.; Aoki, M.; Matsumoto, M.; Towata, S.-I.; Li, H.-W.; Orimo, S.-I. Synthesis and Crystal Structure Analysis of Complex Hydride  $\text{Mg}(\text{BH}_4)(\text{NH}_2)$ . *Int. J. Hydrogen Energy* **2013**, *38*, 6730–6735.